

# X-ray spectral states and metallicity in the ultraluminous X-ray sources NGC 1313 X-1 and X-2

Fabio Pintore<sup>1,2</sup> & Luca Zampieri<sup>2</sup>

<sup>1</sup> *Dipartimento di Astronomia, Università di Padova, Vicolo dell'Osservatorio 3, I-35122 Padova, Italy*

<sup>2</sup> *INAF-Osservatorio Astronomico di Padova, Vicolo dell'Osservatorio 5, I-35122 Padova, Italy*

Accepted ... Received ...; in original form ...

## ABSTRACT

We present a systematic analysis of the X-ray spectra of NGC 1313 X-1 and NGC 1313 X-2, using three years of *XMM-Newton* observations. We fitted the continuum with a Comptonization model plus a multicolor blackbody disc, that describes the effects of an accretion disc plus a corona. We checked the consistency of this spectral model on the basis of the variability patterns of its spectral parameters. We found that the two sources show different spectral states. We tentatively interpret the observed behaviour of NGC 1313 X-1 and X-2 within the framework of near Eddington and/or super-Eddington accretion. We also attempted to determine the chemical abundances in the local environment of NGC 1313 X-1 and X-2 from the EPIC and RGS spectra. The results appear to indicate subsolar metallicity for both sources.

**Key words:** accretion, accretion discs – X-rays: binaries – X-rays: galaxies – X-rays: individuals (NGC 1313 X-1, NGC 1313 X-2)

## 1 INTRODUCTION

Ultra luminous X-ray sources (ULXs) are extragalactic, point-like, off nuclear X-ray sources with observed isotropic X-ray luminosities higher than the Eddington luminosity for accretion onto a  $10 M_{\odot}$  black hole, and typically in the range from  $10^{39}$  erg s<sup>−1</sup> up to  $\sim 10^{41}$  erg s<sup>−1</sup> (e.g. Fabbiano 1989). Several pieces of observational evidence strongly suggest that the majority of ULXs are accreting black hole (BH) X-ray binaries (XRBs) with massive donors (e.g. Zampieri & Roberts 2009 and references therein).

At present, the size and the origin of the BHs hosted in ULXs is still a matter of debate. It has been proposed that ULXs are powered by a stellar mass BHs ( $10\div 20 M_{\odot}$ ) accreting largely above the Eddington limit and/or having beamed emission (e.g. King et al. 2001; King 2009; Begelman 2006; Socrates & Davis 2006; Poutanen et al. 2007). Alternatively, the compact object could simply be bigger, and the accretion would be in the usual sub-Eddington regime. In this case the compact object would be an intermediate mass black hole (IMBH) with a mass in excess of  $100 M_{\odot}$  (e.g. Colbert & Mushotzky 1999). Another interpretation follows from the possibility of forming massive stellar remnant BHs ( $20\div 80 M_{\odot}$ ) from the direct collapse of low-metallicity, massive ( $\gtrsim 30 - 40 M_{\odot}$ ) stars (Fryer 1999; Belczynski et al. 2010). Some ULXs may contain such massive stellar remnant BHs accreting at or slightly above the Eddington rate, formed in low metallicity environments ( $Z \sim 0.1 Z_{\odot}$ ; e.g. Zampieri & Roberts 2009; Mapelli et al. 2009, 2010).

The spectra of many ULXs are qualitatively similar to those of Galactic XRBs, and can be well reproduced by a multicolour disc blackbody with a low characteristic temperature ( $\sim 0.1 - 0.4$  keV),

plus a power-law continuum with a spectral index  $\sim 1.5 - 2.5$  (e.g. Feng & Kaaret 2005). The high luminosity and low temperature of the disc component were interpreted as supporting evidence for the existence of IMBHs (Miller et al. 2003, 2004). However, in the last few years, *Chandra* and *XMM-Newton* observations revealed new behaviours, showing the existence of X-ray spectra with rather peculiar properties. For some of the brightest ULXs, equally acceptable fits of their spectra may be obtained with (physically) different models, that suggest the presence of an optically thick corona, a fast ionized outflow or a slim disc (e.g. Stobbart et al. 2006; Gonçalves & Soria 2006; Mizuno et al. 2007). Recently, Gladstone et al. (2009) have shown that disc plus Comptonized corona models fit the data of the highest quality *XMM-Newton* spectra of several ULXs well, suggesting that the corona is cool and optically thick.

In order to increase our understanding of ULXs and shed light on the mechanism at the origin of their powerful emission, it is crucial to investigate the evolution of their accretion flow through the variability of their X-ray spectra. In this work we present a systematic analysis of the X-ray spectra of two ULXs in the galaxy NGC 1313, using three years of *XMM-Newton* observations. The barred spiral galaxy NGC 1313 hosts three ULXs, one of which (NGC 1313 X-3) is a known supernova (SN 1978K) interacting with the circumstellar medium. The other two ULXs, NGC 1313 X-1 and X-2 (X-1 and X-2 hereafter), are located in different positions, close to the nucleus ( $\sim 50''$ ) X-1 and at the outskirts of the host galaxy ( $\sim 6'$ ) X-2. NGC 1313 has been observed several times over the years by *XMM-Newton* and a sufficient number of X-ray spectra are now available to attempt a characterization of the spectral variability of the sources hosted in it.

Feng & Kaaret (2006) fitted a sequence of 12 *XMM-Newton*

**Table 1.** Log of the observations.

No.	Obs ID	Date	Exp <sup>a</sup> (ks)	Instr. (X-1) <sup>b</sup>	Instr. (X-2) <sup>b</sup>	Net counts(X-1)	Net counts(X-2)
1	0150280101	11/25/2003	1	M1/M2	M1/M2/pn	651, 637	578, 643, 734
2	0150280301	12/21/2003	7.4	pn	M1/M2/pn	7648	2960, 2874, 6304
3	0150280401	12/23/2003	3.2	pn	M1/M2/pn	2223	2215, 2151, 3030
4	0150280501	12/25/2003	1.7	pn	M1/M2/pn	484	1379, 1378, 904
5	0150280601	01/08/2004	6.5	pn	M1/M2/pn	5524	2714, 1694, 1690
6	0150281101	01/16/2004	2.7	M1/M2/pn	M1/M2/pn	1770, 1993, 2366	887, 713, 1013
7	0205230201	05/01/2004	7.8 <sup>c</sup>	M1/M2	M1/M2	1310, 1489	700, 783
8	0205230301	06/05/2004	8.7	M1/M2/pn	M1/M2/pn	5446, 5151, 8685	3800, 3798, 819
9	0205230401	08/23/2004	3.8	M1/M2/pn	M1/M2/pn	2397, 2643, 2323	1252, 1316, 1173
10	0205230501	11/23/2004	12.5	M1/M2	M1/M2/pn	3013, 3179	1523, 1594, 4164
11	0205230601	02/07/2005	9.0	M1/M2/pn	M1/M2/pn	5025, 2435, 2187	3702, 3697, 8224
12	0301860101	03/06/2006	17.2	pn	M1/M2/pn	3980	4043, 4374, 11426
13	0405090101	10/16/2006	78.6	M1/M2/pn	pn	24277, 25141, 58116	53271

<sup>a</sup> GTI of EPIC-pn<sup>b</sup> pn = EPIC-pn camera; M1/M2 = EPIC-MOS1/MOS2 camera<sup>c</sup> GTI of EPIC-MOS

observations of X-1 and X-2 with a power-law plus multicolor disc blackbody model and found an anti-correlation between the luminosity and the inner temperature of the MCD component. For this reason they concluded that such component does not originate in a standard accretion disc. The optical and X-ray variability of X-2 was also investigated by Mucciarelli et al. (2007) to constrain the properties of the donor star and the binary system. They found that the power-law component hardens as the flux increases, opposite to what usually shown by Galactic BH XRBs.

Another crucial issue related to ULX formation are the properties of the environment in which ULXs are embedded. Claims regarding the correlation of ULXs with low metallicity environments have been recently reported. Swartz et al. (2008) found that within the Local Volume the specific ULX frequency decreases with host galaxy mass above  $\sim 10^{8.5} M_{\odot}$ , meaning that smaller, lower metallicity systems have more ULXs per unit mass than larger galaxies. Mapelli et al. (2009) and Zampieri & Roberts (2009) suggested that at least a fraction of ULXs may be powered by massive stellar BHs formed from the direct collapse of low-metallicity massive stars. Using binary synthesis calculations, Linden et al. (2010) proposed another interpretation, in which the number, the lifetime and (to a less extent) the luminosity of high mass XRBs are enhanced at low metallicities. Only few measurements of the metallicity in the ULX environment are available, and results are not conclusive (see e.g. Zampieri & Roberts 2009 and references therein). While optical observations provide probably the best means to perform such measurements, also the abundances inferred from the detection of K-shell photoionization edges of intermediate mass or heavy elements in the X-ray absorption spectrum of ULXs can be a viable tool, if high signal-to-noise spectra are available. This was already attempted by Winter et al. (2007) for a sample of 14 ULXs with *XMM-Newton* spectra, obtaining values that match the solar abundance, but no further investigation, especially using the high resolution RGS spectra, has been attempted since then.

In this work we try to characterize the spectral variability of X-1 and X-2 using all the available *XMM-Newton* data. Recently, detailed spectral variability analyses were performed by Feng & Kaaret (2009) and Kajava & Poutanen (2009) on *XMM-Newton* and *Chandra* data of some ULXs, by Dewangan et al. (2010) on the last two *XMM-Newton* observations of NGC 1313 X-1, and by

Vierdayanti et al. (2010) on *XMM-Newton* and Swift data of Ho IX X-1. We will try to constrain also the metallicity of the absorbing gas towards X-1 and X-2 using the RGS and EPIC spectra of the longest observation, and stacking together all the RGS observations. Some preliminary results of this investigation were reported in Pintore & Zampieri (2011). Because of some improvements in the present analysis, the results and interpretation reported here supersede our previous ones. The plan of the paper is the following. In § 2 we summarize the data selection and reduction procedures, while in § 3 and § 4 we present our results and discuss them in § 5.

## 2 DATA REDUCTION

We re-analyzed all the available *XMM-Newton* spectra of the two ULXs hosted in the spiral galaxy NGC 1313, X-1 and X-2, with homogeneous criteria. The 17 observations span a time interval of six years, from 17 October 2000 to 16 October 2006, but three observations were excluded because of high flares contamination. Also the observation of October 2000 was excluded from the analysis because the calibration before December 2000 may be incomplete. Data were reduced using SAS v. 9.0.0. EPIC-MOS and EPIC-pn spectra were extracted selecting the good time intervals with a background count rate not higher than  $0.45 \text{ count s}^{-1}$  in the energy range 10 – 12 keV. We set ‘FLAG=0’ in order to exclude the events at the CCD edge and the bad pixels. Spectra were extracted from events with *PATTERN*  $\leq 4$  for EPIC-pn (which allows for single and double pixel events) and *PATTERN*  $\leq 12$  for EPIC-MOS (which allows for single, double, triple and quadruple pixel events). We used 35" and 30" circular extraction regions for X-1 and X-2, respectively. For the background we chose a 65" extraction circular region on the same CCD chip where the source is located. If the sources were on or near a CCD gap, no spectra were extracted. For X-2 the off-axis angle is quite similar for most of the observations (not much larger than  $0.4'$  for all but three observations). For X-1, 10 observations have off-axis angles that differ no more than  $1'$ , while the remaining three show a more significant variation. However, their spectra do not seem to present any peculiarity possibly associated to variations in the fraction of encircled energy. RGS spectra were extracted using the *rgsproc* task with the

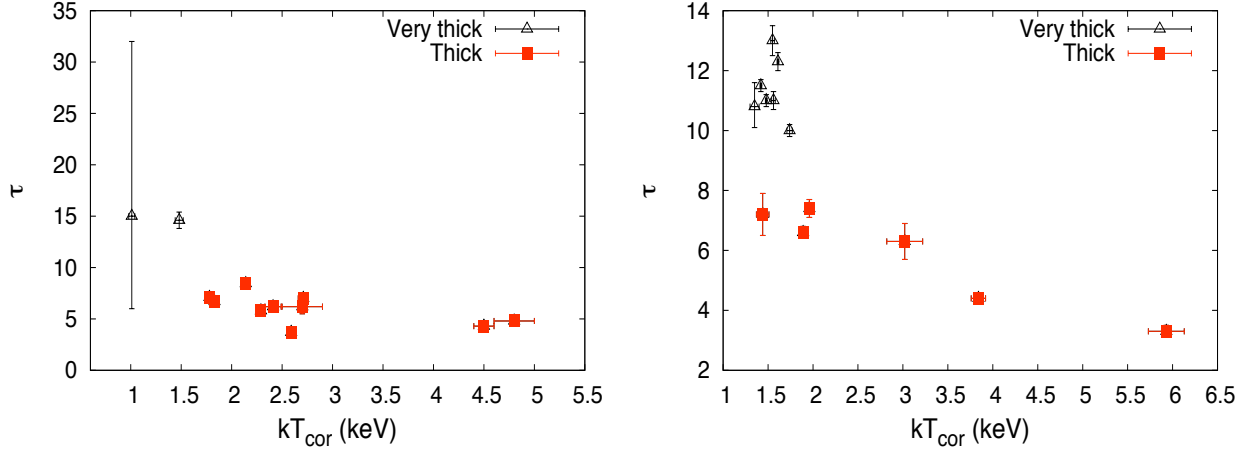


**Figure 1.** Optical depth  $\tau$  versus temperature of the corona  $kT_{cor}$  for the X-ray spectral fits of X-1 (left) and X-2 (right) with a *diskbb+comptt* model. Observations that have a very thick corona are represented with *black* triangles while observations with a thick corona are represented as *red* squares.

option *spectrumbinning=lambda*. In this way it turns out to be possible to combine the spectra of different observations. The EPIC spectra were grouped with a minimum of 25 counts per channel, while RGS spectra with 50 counts per channel.

All the spectral fits were performed using XSPEC v. 12.5.1. To improve the counting statistics, whenever possible, we fitted the EPIC-pn and EPIC-MOS spectra simultaneously. EPIC spectral fits were performed in the 0.3–10.0 keV energy range, while RGS fits were limited to the 0.45–2.0 keV energy range. For each instrument, a multiplicative constant was introduced to account for possible residual differences in the instrument calibrations. The constant of the EPIC-pn data set was fixed equal to 1, while the other two are allowed to vary. In general, the differences among the three instruments are not higher than 10%.

### 3 X-RAY SPECTRAL FITS

#### 3.1 Comptonization plus multicolor blackbody disc

We analyzed 13 out of the 17 *XMM-Newton* observations of X-1 and X-2 adopting an absorbed multicolor blackbody disc plus Comptonization component, modelled with *diskbb+comptt* (Mitsuda et al. 1984; Titarchuk 1994) in XSPEC. This model was successfully adopted in previous investigations to describe phenomenologically the spectra of ULXs (Stobbart et al. 2006; Gladstone et al. 2009; Feng & Kaaret 2009). Although several of our observations show acceptable fits using only the *comptt* component, in some cases adding the *diskbb* component leads to a significant improvement in the fit. Therefore, in order to perform a comparison within the framework of a unique spectral model, here we assume the *diskbb+comptt* as reference model for all the observations and check its consistency on the basis of the variability patterns of its spectral parameters. The interstellar absorption was modelled with the *tbabs* model in XSPEC. We fixed the Galaxy column density along the line of sight at  $3.9 \times 10^{20} \text{ cm}^{-2}$  (Dickey et al. 1990) and added a free absorption component to model the local absorption near the source.

The results of the spectral fits with the *diskbb+comptt* model for the 13 *XMM-Newton* observations of X-1 and X-2 are reported in Table 2. We tied the temperature of the disc ( $T_{disc}$ ) to that of the

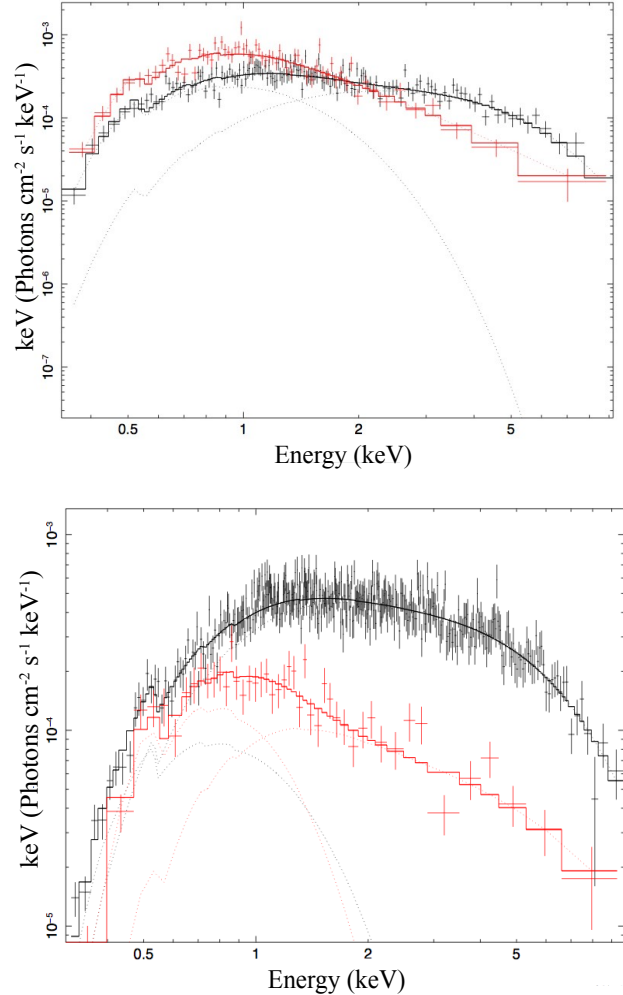


**Figure 2.** X-ray spectra (energy  $\times$  photons) of X-1 (top) and X-2 (bottom) for observations that have a very thick corona (*black*) and a thick corona (*red*). In both cases the comparison is between observations #9 and #12, respectively.

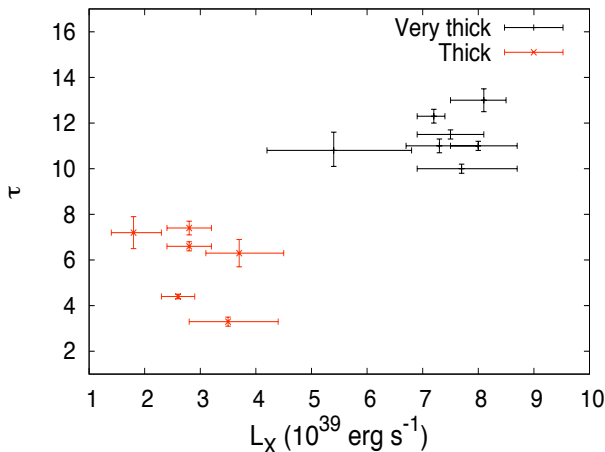
**Table 2.** Best fitting spectral parameters of NGC1313 X-1 and X-2 in different observations obtained with the absorbed *diskbb+comptt* model.

NGC1313 X-1								
No.	Date	$N_H^a$ ( $10^{21}$ cm $^2$ )	$kT_{disc}^{b,c}$ (keV)	$kT_{cor}^d$ (keV)	$\tau^e$	$L_X$ [0.3-10 keV] <sup>f</sup> ( $10^{39}$ erg s $^{-1}$ )	$L_{disc}$ [0.3-10 keV] <sup>g</sup> ( $10^{39}$ erg s $^{-1}$ )	$\chi^2/dof$
1	11/25/2003	$0.2^{+0.2}_{-0.2}$	$0.80^{+0.01}_{-0.01}$	$9.03^{+400}_{-5}$	$16.2^{+2}_{-2}$	$10.0^{+0.3}_{-0.3}$	$5.0^{+1.2}_{-0.4}$	21.33/38
2	12/21/2003	$1.9^{+0.1}_{-0.1}$	$0.199^{+0.005}_{-0.005}$	$1.83^{+0.02}_{-0.02}$	$6.7^{+0.1}_{-0.1}$	$11.5^{+0.9}_{-0.9}$	$0^{+3e36}_{-0}$	195.47/226
3	12/23/2003	$4.0^{+0.2}_{-0.2}$	$0.229^{+0.004}_{-0.004}$	$2.41^{+0.08}_{-0.08}$	$6.2^{+0.3}_{-0.3}$	$14.2^{+2.5}_{-2.2}$	$4.6^{+0.8}_{-0.9}$	64.38/75
4	12/25/2003	$4.3^{+0.4}_{-0.4}$	$0.179^{+0.005}_{-0.005}$	$2.7^{+0.2}_{-0.2}$	$6.2^{+0.7}_{-0.7}$	$14.9^{+5.9}_{-4.8}$	$6.6^{+2.4}_{-2.4}$	12.88/12
5	01/08/2004	$2.7^{+0.1}_{-0.1}$	$0.244^{+0.003}_{-0.003}$	$4.5^{+0.1}_{-0.1}$	$4.3^{+0.2}_{-0.2}$	$10.8^{+1.3}_{-1.1}$	$2.7^{+0.4}_{-0.3}$	184.56/176
6	01/16/2004	$1.3^{+0.1}_{-0.1}$	$0.226^{+0.006}_{-0.006}$	$2.28^{+0.04}_{-0.04}$	$5.8^{+0.1}_{-0.1}$	$9.3^{+1.8}_{-0.6}$	$0^{+6e38}_{-0}$	194.71/197
7	05/01/2004	$3.2^{+0.2}_{-0.2}$	$0.216^{+0.003}_{-0.003}$	$4.8^{+0.2}_{-0.2}$	$4.8^{+0.3}_{-0.3}$	$8.0^{+1.8}_{-1.3}$	$2.4^{+0.6}_{-0.4}$	100.97/91
8	06/05/2004	$1.87^{+0.07}_{-0.07}$	$0.242^{+0.003}_{-0.003}$	$1.78^{+0.02}_{-0.02}$	$7.1^{+0.1}_{-0.1}$	$15.0^{+1}_{-1}$	$1.3^{+0.2}_{-0.2}$	511.38/543
9	08/23/2004	$2.3^{+0.1}_{-0.1}$	$0.158^{+0.002}_{-0.002}$	$2.59^{+0.03}_{-0.03}$	$3.70^{+0.07}_{-0.07}$	$5.4^{+0.6}_{-0.5}$	$0^{+4e38}_{-0}$	233.91/232
10	11/23/2004	$2.2^{+0.1}_{-0.1}$	$0.367^{+0.003}_{-0.003}$	$1.48^{+0.04}_{-0.04}$	$14.6^{+0.8}_{-0.8}$	$8.2^{+1}_{-0.9}$	$3.7^{+0.3}_{-0.3}$	165.41/184
11	02/07/2005	$2.91^{+0.09}_{-0.09}$	$0.208^{+0.002}_{-0.002}$	$2.71^{+0.05}_{-0.05}$	$7.0^{+0.2}_{-0.2}$	$8.9^{+1}_{-1}$	$2.7^{+0.3}_{-0.3}$	313.10/305
12	03/06/2006	$2.3^{+0.1}_{-0.1}$	$0.459^{+0.004}_{-0.004}$	$1.01^{+0.03}_{-0.03}$	$15^{+7}_{-9}$	$4.6^{+0.6}_{-0.5}$	$2.5^{+0.1}_{-0.2}$	168.29/139
13	10/16/2006	$2.67^{+0.002}_{-0.002}$	$0.222^{+0.001}_{-0.001}$	$2.14^{+0.01}_{-0.01}$	$8.44^{+0.06}_{-0.06}$	$7.1^{+0.2}_{-0.2}$	$2.1^{+0.1}_{-0.1}$	1490.95/1420

NGC1313 X-2								
No.	Date	$N_H^a$ ( $10^{21}$ cm $^2$ )	$kT_{disc}^b$ (keV)	$kT_{cor}^c$ (keV)	$\tau^d$	$L_X$ [0.3-10 keV] <sup>e</sup> ( $10^{39}$ erg s $^{-1}$ )	$L_{disc}$ [0.3-10 keV] <sup>f</sup> ( $10^{38}$ erg s $^{-1}$ )	$\chi^2/dof$
1	11/25/2003	$0.6^{+0.2}_{-0.2}$	$0.44^{+0.01}_{-0.01}$	$1.35^{+0.05}_{-0.05}$	$10.8^{+0.8}_{-0.7}$	$5.4^{+1.4}_{-1.2}$	$12^{+3}_{-4}$	58.72/62
2	12/21/2003	$1.6^{+0.1}_{-0.1}$	$0.380^{+0.004}_{-0.004}$	$1.56^{+0.02}_{-0.02}$	$11.0^{+0.3}_{-0.3}$	$7.3^{+0.7}_{-0.6}$	$14^{+1}_{-2}$	386.05/395
3	12/23/2003	$0.5^{+0.1}_{-0.1}$	$0.27^{+0.01}_{-0.01}$	$1.74^{+0.03}_{-0.03}$	$10.0^{+0.2}_{-0.2}$	$7.7^{+1}_{-0.8}$	$0^{+6e+37}_{-0}$	245.35/248
4	12/25/2003	$1.2^{+0.2}_{-0.2}$	$0.469^{+0.006}_{-0.006}$	$3.02^{+0.2}_{-0.2}$	$6.3^{+0.6}_{-0.6}$	$3.7^{+0.8}_{-0.6}$	$14.4^{+2}_{-8}$	99.68/120
5	01/08/2004	$1.4^{+0.1}_{-0.1}$	$0.266^{+0.005}_{-0.005}$	$1.89^{+0.04}_{-0.04}$	$6.6^{+0.2}_{-0.2}$	$2.8^{+0.4}_{-0.4}$	$4.5^{+1}_{-0.9}$	175.27/201
6	01/16/2004	$2.1^{+0.2}_{-0.2}$	$0.186^{+0.005}_{-0.005}$	$5.93^{+0.2}_{-0.2}$	$3.3^{+0.2}_{-0.2}$	$3.5^{+0.7}_{-0.5}$	$4.7^{+2.3}_{-1.7}$	84.94/85
7	05/01/2004	$1.0^{+0.3}_{-0.3}$	$0.38^{+0.01}_{-0.01}$	$1.44^{+0.07}_{-0.07}$	$7.2^{+0.2}_{-0.2}$	$1.8^{+0.7}_{-0.4}$	$6.3^{+1.7}_{-1.4}$	55.41/46
8	06/05/2004	$1.1^{+0.1}_{-0.1}$	$0.238^{+0.006}_{-0.006}$	$1.48^{+0.01}_{-0.01}$	$11.0^{+0.2}_{-0.2}$	$8.0^{+0.7}_{-0.5}$	$0^{+4e39}_{-0}$	514.96/507
9	08/23/2004	$3.0^{+0.1}_{-0.1}$	$0.208^{+0.002}_{-0.002}$	$1.96^{+0.05}_{-0.05}$	$7.4^{+0.3}_{-0.3}$	$2.8^{+0.4}_{-0.4}$	$12^{+2}_{-2}$	150.72/131
10	11/23/2004	$2.3^{+0.1}_{-0.09}$	$0.226^{+0.002}_{-0.002}$	$3.84^{+0.08}_{-0.08}$	$4.4^{+0.1}_{-0.1}$	$2.6^{+0.3}_{-0.3}$	$7.0^{+1.1}_{-0.9}$	210.89/237
11	02/07/2005	$1.69^{+0.09}_{-0.08}$	$0.633^{+0.004}_{-0.004}$	$1.55^{+0.02}_{-0.02}$	$13.0^{+0.5}_{-0.5}$	$8.1^{+0.4}_{-0.6}$	$28^{+2}_{-1}$	490.92/486
12	03/06/2006	$1.54^{+0.08}_{-0.08}$	$0.288^{+0.006}_{-0.006}$	$1.42^{+0.01}_{-0.01}$	$11.5^{+0.2}_{-0.2}$	$7.5^{+0.6}_{-0.6}$	$5.1^{+1}_{-0.9}$	577.03/603
13	10/16/2006	$1.89^{+0.04}_{-0.04}$	$0.61^{+0.02}_{-0.02}$	$1.61^{+0.01}_{-0.01}$	$12.3^{+0.3}_{-0.3}$	$7.2^{+0.2}_{-0.3}$	$28^{+1.1}_{-0.2}$	841.83/854

<sup>a</sup> Column density; <sup>b</sup> Inner disc temperature; <sup>c</sup> The seed photons temperature  $T_0$  is assumed to be equal to  $T_{disc}$ . <sup>d</sup> Temperature of the corona; <sup>e</sup> Optical depth of the corona; <sup>f</sup> Unabsorbed total x-ray luminosity in the 0.3 -10 keV range; <sup>g</sup> Unabsorbed disc luminosity in the 0.3-10 keV range.

**Figure 3.** Optical depth  $\tau$  versus unabsorbed total luminosity (in the 0.3-10 keV range) for X-2. The black points represent the very thick corona state while the red crosses are the thick corona state.

seed photons ( $T_0$ ) for comptonization. We will comment on this choice at the end of this Section. The reported errors are at the 90% confidence level for one interesting parameter. We noted that there are often several local minima with close values of the  $\chi^2$ , sometimes with evidence for both a strong/warm and a weak/cool (or no) disc. After a careful inspection of the  $\chi^2$  surface, we found the absolute minima for each observation reported in Table 2. However, one should be aware that the actual uncertainty on the disc parameters caused by the topology of the  $\chi^2$  surface is at least a few times larger than the formal error reported in the Table. We tried to adopt also more physical models, such as the *eqtherm* (Coppi 2001) and the *DKBBFTH* (Done & Kubota 2006). We found that the counting statistics of most of the spectra is inadequate to constrain the parameters of *eqtherm* and *DKBBFTH* (see also below).

The longest observation of X-1 has a short segment of  $\sim 3.5$  ks within the first 13 ks that shows some intrinsic variability (a slight systematic hardening at high energies) and was then removed from the analysis. We note also that observation #1 has a very low value of  $N_H$  compared to the other observations and a low counting statistics. It converges towards a local minimum with a very strong

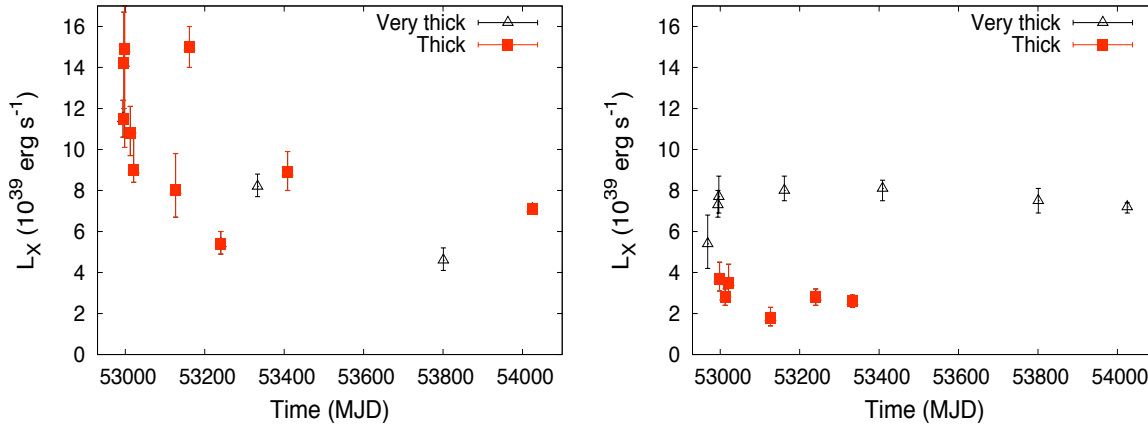


**Figure 4.** X-ray unabsorbed luminosity evaluated in the 0.3-10 keV energy band (a distance of 3.7 Mpc was assumed; Tully 1988) for all the *XMM-Newton* observations of X-1 (up-left) and X-2 (up-right). Observations with a very thick corona are represented with black triangles while observations with thick corona are represented as red squares. All the (unabsorbed) luminosities are evaluated in the 0.3-10 keV energy band.

disc component and with parameters unlike those of all the other spectra. For this reason, we excluded it from the following analysis.

Figure 1 shows a plot of the optical depth  $\tau$  versus the temperature of the corona  $kT_{cor}$  obtained from the best fits of both sources. There appears to be well defined loci in the  $kT_{cor}$ - $\tau$  plane, indicating the existence of a somewhat ordered behaviour in the spectral variability of the corona. The spectra of X-2 populate two distinct regions characterized by very large optical depths ( $\tau \gtrsim 10$ ) and low temperatures ( $kT_{cor} \sim 1.5$  keV), on one side, and smaller optical depths ( $\tau \lesssim 8$ ) and a range of temperatures ( $kT_{cor} \sim 1.5$ -6 keV), on the other side. In both cases the corona turns out to be optically thick. In the following we refer to these two regions as “very-thick” and “thick” corona states, respectively. X-1 may also be interpreted within the same framework. An analysis of the X-ray flux variability shows that both sources tend to be significantly more variable when the coronae are thicker (fractional variability  $\gtrsim 9$ -10%, see table 3), which would strengthen the analogies between their behaviours. However, the clustering of the observations in the  $kT_{cor}$ - $\tau$  plane of X-1 is not so well defined and the region with high optical depths is populated by only two observations. Furthermore, although not included in Figure 1 because of the low counting statistics, our interpretation is not consistent with the spectral parameters inferred from observation #1. So, present data are not sufficient to establish whether X-1 has indeed a bi-modal behaviour similar to that shown by X-2 or the changes in the optical depth should be interpreted in a different way (e.g. as due to different variability patterns or accretion geometries; Feng & Kaaret 2006; Dewangan et al. 2010). In the following we will continue to distinguish between the observations of X-1 with a very thick corona ( $\tau \gtrsim 10$ ) and a thick corona ( $\tau \lesssim 8$ ), being aware that they may represent physically different states with respect to those of X-2.

An example of the spectral shapes when the two sources are in different positions on the  $kT_{cor}$ - $\tau$  plane is shown in Figure 2. Again there are analogies and differences between X-1 and X-2. In both cases the spectra for very high coronal depths are bell-shaped, with a clear turn-over at  $\gtrsim 3$ –4 keV (e.g. Stobbart et al. 2006), whereas the spectra in the low- $\tau$  region are steeper and do not show strong evidence of curvature at high energies. Only for X-2 the two spectral states appear to correlate with total luminosity, the very-thick

corona state being more luminous (see Figure 3). In X-1 there is no significant dependence of the spectral shape on  $L_X$ . This is evident also from the behaviour of the spectra shown in Figure 2. While for X-2 the thick corona spectra stay always below those in the very thick corona state, for X-1 there is a sort of crossing/pivoting point of the observed spectra (see also Kajava & Poutanen 2009) at  $\sim 2$  keV. Therefore, the total counts in the thick corona state of X-2 are clearly smaller than those in the very thick corona state, while in X-1 the deficit of photons observed at low energies in spectra with larger optical depths is compensated by the excess of photons at high energies. Figure 4 shows the light curves of X-1 and X-2 computed from the best fitting *diskbb+comptt* model (a distance of 3.7 Mpc was assumed; Tully 1988). On average, X-1 has a luminosity ( $\sim 10^{40}$  erg s $^{-1}$ ) higher than that of X-2 ( $\sim 5 \times 10^{39}$  erg s $^{-1}$ ). Variability of a factor  $\sim 3$  and  $\sim 5$  is observed for X-1 and X-2, respectively. We further investigated the behaviour of the soft component in both sources. The discs are soft or warm, with temperatures of  $\sim 0.2$ –0.5 keV for X-1 and  $\sim 0.2$ –0.6 keV for X-2. Three spectra of X-1 are consistent with zero normalization (or absence) of the soft component. In eight observations the luminosity of the soft component is  $\sim 10^{39}$  erg s $^{-1}$  and it represents a significant fraction of the total flux ( $\gtrsim 30\%$ ). Excluding the spectral fits that return zero normalization of the soft component, there is no evidence of correlation or anti-correlation between the disc (or total) luminosity and the inner disc temperature. In X-2 the luminosity of the soft component is a significant fraction ( $\gtrsim 30\%$ ) of the total luminosity in six observations. Two observations have normalization consistent with zero. Excluding them, the disc luminosity appears to show a weak power-law correlation with the inner temperature,  $L_{disc} \propto T_{disc}^{1.2 \pm 0.3}$ . However, the correlation is uncertain, as the two observations that substantiate it (those with higher  $kT_{disc}$ ) have also rather shallow minima in  $\chi^2$ , admitting both a strong/warm and a weak/cool disc fit with close values of the  $\chi^2$ . No correlation is found using the total luminosity.

### 3.2 Effects of varying the ratio of seed photons temperature to the disc temperature

The comptonizing coronae of the *comptt* model turn out to be optically thick. This poses a problem, as in these physical conditions

**Table 3.** Fractional variability of NGC 1313 X-1 and X-2.

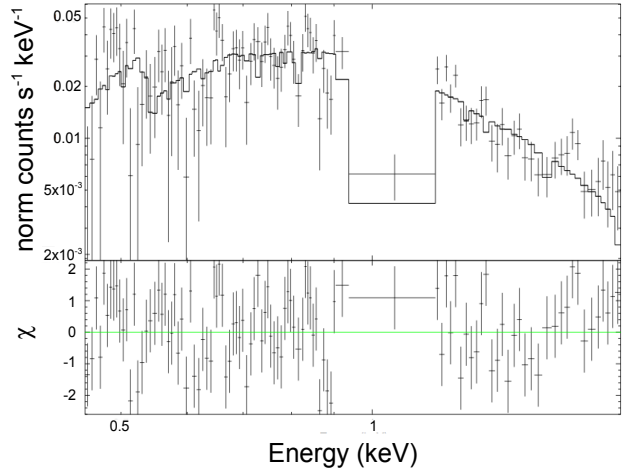
<i>Very Thick corona</i>				
Energy band <sup>a</sup>	X-2 (Obs. 13) counts s <sup>-1</sup>	$F_{var}$ (per cent) <sup>b</sup>	X-1 (Obs. 12) <sup>c</sup> counts s <sup>-1</sup>	$F_{var}$ (per cent) <sup>b</sup>
0.2-10 keV	$0.978 \pm 0.005$	$9.77 \pm 0.07$	$1.47 \pm 0.09$	$14.6 \pm 0.6$
<i>Thick corona</i>				
Energy band <sup>a</sup>	X-2 (Obs. 10) counts s <sup>-1</sup>	$F_{var}$ (per cent) <sup>b</sup>	X-1 (Obs. 13) <sup>c,e</sup> counts s <sup>-1</sup>	$F_{var}$ (per cent) <sup>b</sup>
0.2-10 keV	$0.377 \pm 0.006$	$< 9.3^d$	$0.77 \pm 0.07$	$2.3^{+0.9}_{-1.9}$

<sup>a</sup> The adopted energy band is for a direct comparison with Dewangan et al. (2010) <sup>b</sup> Calculated from the background subtracted EPIC-pn light curve, with 200 s time bins. <sup>c</sup> From Dewangan et al. (2010). <sup>d</sup> 3  $\sigma$  upper limit. <sup>e</sup> Fractional variability computed for the whole observation, including the short segment of 3.5 ks that we left out from the spectral analysis.

the disc underneath the corona is masked by it. Therefore, the temperature of the disc component refers to the outer visible part of the disc, while the temperature of the seed photons  $T_0$  is not necessarily equal to  $T_{disc}$ . For this reason, Gladstone et al. (2009) adopted the *DKBBFTH* model in which the corona is assumed to cover the inner disc. We tried to apply the same model to our spectral sequence, but found that it converges to plausible physical values of the parameters only for the highest quality spectra. We then tried to repeat our analysis with the *diskbb+comptt* model and disconnecting the two temperatures, but this leads to difficulties in finding a global minimum (see also the analysis of NGC 5204 X-1 in Feng & Kaaret 2009). Finally, we decided to test our results tying the two temperatures with a fixed proportionality constant.

If the corona is optically thick and is absorbing a constant fraction  $f$  of the accretion power, the actual inner disc temperature  $T'_1$  is lower than the inner temperature of the disc in absence of the corona  $T_1$ , as  $T'_1 = T_1(1 - f)^{1/4}$  (e.g. Gladstone et al. 2009). If  $R_1$  and  $R_T$  are the inner disc radius and the truncation radius of the corona respectively, from the relation  $T(R) \approx T_1(R/R_1)^{-3/4}$ , valid for a disc in absence of the corona, we obtain  $T_1 \approx T_T(R_T/R_1)^{3/4}$ . Thus, we have  $T'_1 \approx T_T(R_T/R_1)^{3/4}(1 - f)^{1/4}$ . Assuming that  $f \lesssim 90\%$  and that the corona is compact ( $R_T \lesssim 4R_1$ ), the inner disc temperature  $T'_1$ , which is also the seed photons temperature, is larger than the temperature of the outer visible disc  $T_T$ , and  $1 \lesssim T'_1/T_T = T_0/T_{disc} \lesssim 2.5$ . We then attempted to perform some additional fits with two fixed values (1.5, 2) of the ratio  $\delta = T_0/T_{disc}$  as representative of this situation.

We found that the spectral fits with a *diskbb+comptt* model and  $\delta = 1.5, 2$  are statistically acceptable and the coronae are still optically thick, with the inferred optical depth weakly depending on  $T_0/T_{disc}$ . The parameters of the corona change by no more than  $\sim 60\%$ , with typical variations of  $\lesssim 20 - 30\%$ . However, the dependence of spectral states on the total luminosity that characterizes the behaviour of X-2 for equal temperatures is lost. For X-1, the temperature of the disc continues to not correlate with the luminosity, as found for equal temperatures. For X-2, varying  $\delta$  the very-thick state becomes less populated, as some observations previously in that state move to the thick corona state. For  $\delta = 1.5$  there is a weak correlation between disc luminosity and temperature ( $L_{disc} \propto T_{in}^{1.4 \pm 0.4}$ ), while if  $\delta = 2$  the correlation disappears. At variance with the correlation found for equal temperatures, the correlation for  $\delta = 1.5$  is not critically dependent only on two observations.

**Figure 5.** Stacked RGS1 spectrum of X-1, along with its best fitting model (see text for details).

These results do not change significantly for slightly more extended coronae. On the other hand, if the corona is very extended and optically thick, the value of  $\delta$  may become so large that the disc component falls essentially outside the *XMM-Newton* band-pass (unless the disc-corona coupling is very strong). In these conditions some spectra are no longer well fitted by the model.

#### 4 CHEMICAL ABUNDANCE ESTIMATES

We analyzed the EPIC-pn and RGS data of all the *XMM-Newton* observations of X-1 and X-2 in an attempt to use them for determining the chemical abundances in the local source environment. Following Winter et al. (2007), for the EPIC-pn 5000 and 40000 counts are necessary to observe the Oxygen K-shell and Iron L-shell absorption edges at 0.538 keV and 0.851 keV, respectively. Observation #13 has  $\sim 58000$  (53000) EPIC-pn counts for X-1 (X-2), and hence we can perform a chemical abundance analysis on the EPIC-pn spectrum similar to that presented in Winter et al. (2007). In the spectral fits the *tbabs* absorption model is replaced with *tbvarabs* that allows to vary the chemical abundances (and grain composition). We set alternatively the abundance of Oxygen or Iron to zero. The spectrum was then fitted with the EPIC contin-



**Table 4.** Abundances inferred from the Oxygen K-shell photoionization edge (0.538 keV) from the X-ray spectral fits of NGC 1313 X-1 and X-2.

NGC 1313 X-1		
	$\tau^a$	$12 + \log(O/H)^b$
RGS (observation 13)	$0.75^{+0.29}_{-0.25}$	$8.7^{+0.1}_{-0.2}$
EPIC (observation 13)	$0.75^{+0.03}_{-0.03}$	$8.72^{+0.02}_{-0.02}$
RGS (stacked)	$0.53^{+0.26}_{-0.23}$	$8.7^{+0.3}_{-0.2}$
NGC 1313 X-2		
	$\tau^a$	$12 + \log(O/H)$
EPIC (observation 13)	$0.46^{+0.05}_{-0.04}$	$8.64^{+0.06}_{-0.05}$

<sup>a</sup> Absorption depth at the threshold energy.

<sup>b</sup> For the solar abundance we assume  $12 + \log(O/H) = 8.92$  ( $Z_{\odot} = 0.02$ ).

uum model in Table 2 (keeping all parameters, but normalizations, fixed) plus an absorption edge, that accounts for the observed absorption feature. The parameters of the edge are then used to compute the abundance.

Using this approach, we found that the O and Fe abundances inferred from the EPIC-pn spectrum of X-1 are consistent with a sub-solar metallicity environment ( $Z \sim 0.6Z_{\odot}$  from the O edge; Table 4). The  $\chi^2$  of the fit with the absorption edge is 1488 for 1423 dof, while that without the edge is 1759 for 1424 dof. For X-2 we find a subsolar abundance for Oxygen ( $Z \sim 0.5Z_{\odot}$ ; see again Table 4) and an Iron abundance consistent with zero. The fits returns  $\chi^2 = 839$  (857 dof) with the O edge and  $\chi^2 = 953$  (858 dof) without it.

We tried to analyze also the RGS data of X-1 and X-2 using the same technique. As the sources are faint, the RGS net count rate is quite low ( $\sim 1.5 \times 10^{-2}$  count s<sup>-1</sup>). Therefore, only the last observation (observation #13, 122 ks) reached a reasonable counting statistics in the RGS for the brightest ULX (X-1), while no useful analysis could be performed on X-2. We tentatively identified two features in absorption in the RGS spectrum of X-1, associated to O I (0.535 keV) and Fe I (0.709 keV). There may be also two other lines in emission at the characteristic energy of O VIII K $\alpha$  (0.653 keV) and Si K $\alpha$  (1.748 keV), but their significance is very low. From the Oxygen edge we found an abundance below solar ( $Z \sim 0.6Z_{\odot}$ ) for the absorbing material towards X-1 (see Table 4), although the statistical improvement obtained including the absorption edge is small.

We tried to improve the analysis stacking together the RGS spectra in such a way to increase the counting statistics. We used only the RGS1 spectra, because our best diagnostic is the Oxygen K-shell photoionization edge at 0.538 keV and the response of the RGS2 has some problems precisely in this energy range (0.5-0.6 keV). The stacked spectra of X-2 have not enough counting statistics for a meaningful analysis. For X-1, we combined spectra together using the *rgscombine* command, that appropriately accounts for the response matrices and backgrounds of the different observations. We had to exclude several observations (#2, 3, 4, 5, 6, 7, 11, 12) that caused technical problems in the processing with XSPEC. Observation #1 was also excluded for the reason explained in the previous Section. The final combined RGS spectrum of X-1 has a total exposure time of 168 ks and  $\sim 2861$  net counts. We fitted it with a *diskbb+comptt* model with parameters fixed and equal to the mean values obtained from the EPIC spectral

fits of X-1, setting the Oxygen abundance to zero and adding an absorption edge (Figure 5). We found that the Oxygen abundance is again subsolar (Table 4). The  $\chi^2$  of the fit with the absorption edge is 139 for 103 dof, while that without the edge is 146 for 104 dof. However, the actual abundance is rather sensitive to the temperature of the soft component and its uncertainty becomes large if  $kT_{disc}$  is included in the spectral fit.

## 5 DISCUSSION

The analysis of all the *XMM-Newton* observations shows that the spectra of X-1 and X-2 can be well reproduced by a Comptonization model plus a soft disc component in which the coronae are always optically thick. Both sources appear to show a well defined behaviour in the optical depth ( $\tau$ ) versus corona temperature ( $kT_{cor}$ ) plane. For X-2 we clearly identified two states that characterize the spectral variability and appear to have also different short term variability properties: a “very-thick” (more variable) corona state in which  $\tau \gtrsim 10$  and  $kT_{cor} \sim 1.5$  keV, and a “thick-corona” state in which  $\tau \lesssim 8$  and  $kT_{cor} \sim 1.5 - 6$  keV. We note that a morphological classification in terms of a harder brighter state and a softer dimmer state, based on a single power-law fit, has already been proposed for X-2 (Feng & Kaaret 2006). Here we offer a physical explanation of these two states in terms of varying parameters of an optically thick corona. The behaviour of X-1 may be interpreted within the same framework but, with presently available data, the observed changes in the coronal optical depth could be explained also in a different way (e.g. as due to different variability patterns or accretion geometries; Feng & Kaaret 2006; Dewangan et al. 2010).

For X-2, which is on average less luminous than X-1, the two spectral states of the corona appear to correlate with luminosity. The optical depth of the corona increases as the total luminosity goes up, as expected if the corona responds rapidly to an increment in the instantaneous accretion rate. The behaviour of the disc component is also different in the two sources. While in X-1 the luminosity and temperature of this component do not correlate, for X-2 we find that  $L_{disc} \propto T_{disc}^{1.2 \pm 0.3}$ . However, as already mentioned, this result is uncertain as the two spectra that substantiate the correlation admit both a strong/warm and a weak/cool disc fit with close values of the  $\chi^2$ .

A spectral analysis based on the assumption that the seed photon temperature ( $T_0$ ) is equal to the disc temperature ( $T_{disc}$ ) has some inconsistencies because, if the corona is optically thick, the innermost part of the accretion disc is actually not visible and, hence, it is not necessarily true that  $T_0 = T_{disc}$ . For this reason, we repeated our analysis with the *diskbb+comptt* model tying the two temperatures with a proportionality constant, that was fixed assuming a compact corona energetically coupled to the disc (disconnecting the two temperatures leads to difficulties in finding a global minimum because of the low counting statistics of several observations). We find changes in the corona parameters of  $\lesssim 60\%$ , with typical variations of  $\lesssim 20 - 30\%$ . However, the dependence of spectral states on the total luminosity that characterizes the behaviour of X-2 for equal temperatures is lost. While for X-1 the temperature of the disc continues not to correlate with the luminosity, for X-2 the correlation persists up to values of  $T_0/T_{disc} \lesssim 1.5$ , consistent with strong disc-corona coupling ( $f \sim 90\%$ ).

We emphasize that the model adopted in the present investigation is not entirely physically consistent. Besides the issues of the relation between  $T_0$  and  $T_{disc}$  that we tried to address as de-

scribed above, there may be other caveats, such as the input photons not being a mono-temperature Wien distribution (as assumed in *comptt*), or the disc structure being different from a standard one at high accretion rates, or the origin and precise location of the thick corona/wind being unknown. However, our purpose was not to adopt the most physically consistent spectral model for ULXs, which does not exist yet, but a simplified one that can reflect the underlying physics and can be tested on the basis of the observed spectral variability patterns, limited by the current data quality.

A full explanation of the observed spectral variability patterns of X-1 and X-2 is beyond the scope of the present investigation and appears not easy. Here we simply propose some interpretations within the framework of recent work on the subject (e.g. Feng & Kaaret 2009; Gladstone et al. 2009; Dewangan et al. 2010; Vierdayanti et al. 2010). X-1 shows higher average isotropic luminosity ( $\sim 10^{40}$  erg s $^{-1}$ ) and smaller variability. The different spectral shapes do not correlate with luminosity, and the temperature and luminosity of the soft component do not vary together. These findings are consistent with X-1 being in the ultraluminous regime (Gladstone et al. 2009), accreting at super-Eddington rates and launching powerful winds from a disc embedded in an optically thick corona. The accretion disc may be there, but in a different physical regime and covered by a wind/corona, while the soft component may actually represent emission from the wind itself. The larger X-ray fractional variability observed when the wind/corona is optically thicker may be consistent with increasing obscuration of the source caused by the turbulent wind itself at higher accretion rates (Middleton et al. 2011a,b).

As far as X-2 is concerned, it behaves in a way similar to X-1 on the  $\tau$ - $kT_{cor}$  plane and also the fractional X-ray variability of the two sources appears to be comparable. Hence the corona may be in a similar physical state. Again, this may be consistent with the picture in which we are seeing the two sources under a high inclination angle and the temporal variability may be produced by blobs in the wind that intersect our line of sight to the hottest central regions of the source (Middleton et al. 2011a,b). However, as noted above, X-2 has a lower average luminosity and, for  $T_0 \lesssim 1.5T_{disc}$ , it shows a weak correlation between the luminosity and inner temperature of the disc component. This may be interpreted as X-2 being in a less extreme regime, in which the average accretion rate is at around or slightly above the Eddington limit. The soft spectral component may then physically represent a true accretion disc which is partly visible and has a characteristic temperature in the range 0.2-0.6 keV. Clearly, some time-dependent interaction between the disc and the corona is likely to occur (e.g. a slight expansion on a dynamical timescale of the corona as the accretion rate increases) and may be responsible for the observed slope of the temperature-luminosity relation ( $L_{disc} \propto T_{disc}^{1.2}$ ), which is different from that of a standard disc with fixed inner radius ( $L_{disc} \propto T_{disc}^4$ ). Clearly, as the corona is always optically thick, it is not possible to use the disc parameters for estimating the BH mass.

We note that the disc temperature-luminosity correlation in X-2 disappears using a simple power-law to describe the spectrum of the corona, as found by Feng & Kaaret (2006) (and by Feng & Kaaret (2009) for IC 342 X-1), probably because the power-law does not take into account the spectral curvature at high energies. The correlation of the optical depth to the corona with luminosity that we found for X-2 (assuming  $T_0 = T_{disc}$ ) is in agreement with the results obtained for Ho IX X-1 by Vierdayanti et al. (2010). Also IC 342 X-1 shows some hint of an increase in the coronal depth as the X-ray luminosity increases (Feng & Kaaret 2009). These similarities in spectral variability patterns appear to be con-

sistent with the proximity of these three ULXs in the spectral sequence proposed by Gladstone et al. (2009).

We used the RGS high spectral resolution to attempt an estimate of the metallicities of the local environments of X-1 and X-2. Because of the low signal-to-noise ratio, only the last, longest observation of X-1 could be used. The analysis was performed also on the EPIC spectrum. The metallicity in the X-1 environment is consistent with being below solar. The last EPIC spectrum of X-2 was also analyzed with the same method and suggests subsolar metallicity. In an attempt to increase the significance of our results we also stacked together the RGS spectra of some observations of X-1 and performed measurements of the metallicity on the stacked spectrum. Also in this case the Oxygen abundance turns out to be below solar, although it is rather sensitive to the temperature of the soft component. Our estimates are in agreement with the abundance measurements from HII regions in NGC 1313 that give values that are all subsolar (Pilyugin 2001; Hadfield et al. 2007; Ripamonti et al. 2010), but are smaller than the slightly supersolar metallicity of the X-1 environment found by Winter et al. (2007). The difference with the latter Authors may be due to the fact that we analyzed an observation with higher counting statistics and adopted a different spectral model.

A couple of ULXs show periodic intensity variations in X-rays which are considered as signatures of the orbital period (Kaaret et al. 2006a,b; Kaaret & Feng 2007; Strohmayer 2009). X-ray spectra seem to change regularly with orbital phase. It is possible that these phase related variations may affect any result obtained from snapshot observations such as those presented here. Furthermore, as mentioned above, the observed spectral variability patterns of X-1 and X-2 are rather complex and their interpretation does not appear directly comparable to that of Galactic XRBs. For these reasons, the acquisition of new, high quality spectra through a dedicated X-ray monitoring programme is definitely needed.

## ACKNOWLEDGEMENTS

We would like to thank Richard Mushotzky for suggesting the stacking of RGS spectra, Chris Done, Tim Roberts and Jeanette Gladstone for helpful remarks on the adopted spectral models, and Emanuele Ripamonti for his suggestions on the metallicity estimates. We thank also the two referees of this paper for useful comments. We acknowledge financial support through INAF grant PRIN-2007-26 and ASI/INAF grant n. I/009/10/0.

## REFERENCES

- Begelman M.C., 2006, ApJ, 643, 1065
- Belczynski K., Bulik T., Fryer C. L., Ruiter A., Valsecchi F., Vink J. S., Hurley J. R., 2010, ApJ, 714, 1217
- Colbert E. J. M., & Mushotzky R. F., 1999, ApJ, 519, 89
- Coppi P.S., 2001, MNRAS
- Dewangan G. C., Misra R., Rao A. R., Griffiths R. E., 2010, MNRAS, 407, 291
- Done C., Kubota A., 2006, MNRAS, 371, 1216
- Dickey J.M., Lockman F.J., 1990, ARA&A, 28, 215
- Fabbiano G., 1989, ARA&A, 27, 87
- Feng H., Kaaret P., 2005, ApJ, 633, 1052
- Feng H., Kaaret P., 2006, ApJ, 650, 75
- Feng H., Kaaret P., 2009, ApJ, 696, 1712
- Fryer C. L., 1999, ApJ, 522, 413



- Gierlinski M., Zdziarski A. A., Poutanen J., Coppi P. S., Ebisawa K., Johnson W. N., 1999, MNRAS, 309, 496  
Gierlinski M., Done C., 2004, MNRAS, 347, 885  
Gladstone J.C., Roberts T.P., Done C., 2009, ApJ, 397, 1836  
Goncalves A.C., Soria R., 2006, MNRAS, 371, 673  
Hadfield L. J., Crowther P.A., 2007, MNRAS, 381, 418  
Kaaret P., Simet M. G., Lang C. C., 2006a, Science 311, 491  
Kaaret P., Simet M. G., Lang C. C., 2006b, ApJ 646, 174  
Kaaret P., Feng H., 2007, ApJ 669, 106  
Kajava J., Poutanen J., 2009, MNRAS, 398, 1450  
King A.R., Davies M. B., Ward M. J., Fabbiano G., Elvis M., 2001, ApJ, 552, L109  
King A. R., 2009, MNRAS, 393, L41  
Linden T., et al. 2010, ApJ, 725, 1984  
Mapelli M., Colpi M., Zampieri L. 2009, MNRAS, 395, L71  
Mapelli M., Ripamonti E., Zampieri L., Colpi M., Bressan A. 2010, MNRAS, 408, 234  
Middleton M.J., Sutton A. D., Roberts, T. P., 2011, MNRAS, tmp,1209  
Middleton M.J., Roberts T.P., Done C., Jackson F.E., 2011, MNRAS, 411, 644  
Miller M. C., Hamilton D. P., 2002, MNRAS, 330, 232  
Miller J. M., Fabbiano G., Miller M. C., Fabian A. C., 2003, ApJ, 585, 37  
Miller J. M., Fabian A. C., Miller M. C., 2004, ApJ, 607, 931  
Mizuno T., et al., PASJ, 59, 257  
Mitsuda K., Inoue H., Koyama K., Makishima K., Matsuoka M., Ogawara Y., Suzuki K., Tanaka Y., Shibasaki N., Hirano T., 1984, PASJ, 36, 741  
Mucciarelli P., Zampieri L., Treves A., Turolla R., Falomo R., 2007, ApJ, 658, 999  
Pilyugin L.S., 2001, A&A, 369, 594  
Pintore F., Zampieri L., 2011, AN, 332, 337  
Poutanen J., et al., 2007, MNRAS, 377, 1187  
Ripamonti E., Mapelli M., Zampieri L., Colpi M.  
Socrates A., & Davis S. W., 2006, ApJ, 651, 1049  
Stobart A. M., Roberts T. P., Wilms J., 2006, MNRAS, 368, 397  
Strohmayer T. E.: 2009, ApJ 706, L210  
Swartz D. A., Soria R., & Tennant A. F., 2008, ApJ, 684, 282  
Titarchuk L., 1994, ApJ, 434, 570  
Tully R. B., 1988, Nearby Galaxies Catalog. Cambridge Univ. Press, Cambridge  
Vierdayanti K., Done, C., Roberts T. P., Mineshige S., 2010, MNRAS, 403, 1206  
Winter L. M., Mushotzky R. F., Reynolds C. S., 2007, Apj, 655, 163  
Zampieri L., Roberts T.P., 2009, MNRAS, 400, 677

This paper has been typeset from a  $\text{\TeX}$ / $\text{\LaTeX}$  file prepared by the author.